ESTIMATION OF PRESSURE AND PERMEABILITY ENHANCEMENT DISTRIBUTION USING INDUCED EARTHQUAKE HYPOCENTER DENSITY FOR THE 2011 PARALANA EGS STIMULATION

Jeremy Riffault[1], David Dempsey[1], Satish Karra[2] and Rosalind Archer[1]

[1] Department of Engineering Science, the University of Auckland, Auckland 1142, New Zealand

[2] Los Alamos National Laboratory, Los Alamos, New Mexico, USA

jrif565@aucklanduni.ac.nz

Keywords: *EGS, Paralana, induced seismicity, injectivity, permeability*

ABSTRACT

To create an Enhanced Geothermal System (EGS), cold water is injected at high pressure, along with acid, with the goal of reactivating pre-existing fractures and enhancing their permeability. Through increases in pore pressure and associated stress changes, shear failure occurs, which is part of the permeability enhancement process, but also results in induced seismicity.

In spite of being the primary goal of stimulation, details about the spatiotemporal evolution of permeability are difficult to determine. One measure of its improvement is the increase in well injectivity, which is defined as the injected flow rate divided by the wellhead pressure. However, this measure is sensitive to both the volume of stimulated rock as well as the permeability increase, and so it does not uniquely constrain the stimulation state. To augment this analysis, we present an inverse modelling approach that incorporates both the injection records and the spatiotemporal distribution of induced seismicity. We present an application of the method to the Paralana-2 EGS stimulation undertaken in 2011 in South Australia.

High pressure injection is modelled by solving coupled flow and heat transport equations in the reservoir simulator FEHM. In the model, the magnitude of permeability increase is a prescribed function of space and time. The injectivity profile observed at Paralana limits the possible set of permeability evolution scenarios, however, additional constraint is necessary to choose amongst these. As induced seismicity is a consequence of elevated pore pressure, we assume that the density of earthquake hypocenters is proportional to pore pressure rise. By comparing the pressure profiles modelled in the different scenarios to the high-resolution microearthquake data collected during the stimulation, we can pick the permeability enhancement distribution scheme most consistent with the injectivity and seismicity data.

1. INTRODUCTION

At Paralana, an EGS project South Australia, a 3964 m deep injection well, named Paralana-2, was drilled in 2009 (Albaric et al., 2014). An injection test designed to enhance in-situ permeability was performed in July 2011. During the first stage, called continuous pumping, 2,200,000 liters of water were injected, accompanied by 110,000 liters of acid at various concentrations, over a period of 3.5 days (Petratherm report, 2012). Later, a propped fracture treatment operation was undertaken, although this step is not considered in this study. Water was injected at 21 °C (Petratherm report, 2012) in formations with a temperature of 190 °C (Albaric et al., 2014). The injection rate was observed to increase approximately linearly, while wellhead pressure was maintained approximately constant (Fig. 1). Injectivity, the ratio of injection rate to wellhead pressure, thus also increases linearly with time. This implies that the permeability of the rock around the wellbore is being enhanced. The physical processes that can increase permeability during such stimulations are: shear failure of existing fractures, either by an increase in pore pressure, changes in the stress field caused by changes in pressure and temperature (porothermoelasticity); or fracture opening through acid injection or thermal contraction.

During the injection, 4753 induced microearthquakes (MEQ) were detected and located. The largest events recorded appear to be approximately located on an inclined plane dipping 13.5° to the SE (Fig. 2).

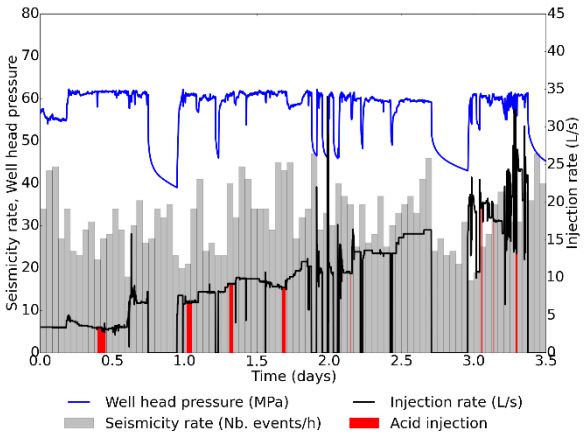

Figure 1: Well head pressure, injection rate, seismicity rate and acid injections recorded during the 2011 hydraulic stimulation conducted in Paralana-2 (modified from Albaric et al., 2014).

We attempt here to get the best estimate of the permeability evolution (location and time) occurring within the 3.5 day stimulation, using available two datasets: wellhead measurements of injectivity and the spatiotemporal distribution of seismicity. We do not model the physical mechanisms responsible for permeability change, but instead use an inverse modelling approach.

We assume that seismic activity reflects subsurface pore pressure increase. Indeed, in a fracture network, a MEQ is a consequence of shear failure of an existing fracture plane. The main cause for shear failure is pressurization, i.e. the increase of fluid pressure within the fracture (Tester et al., 2007). Because of the planar shape of the seismicity cloud, this implies that flow of injected fluid away from the

wellbore is approximately 2D and localized to the inclined structure identified by the seismicity.

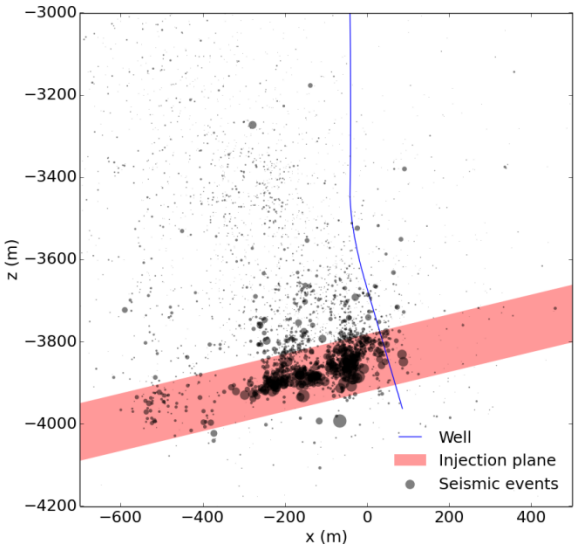

Figure 2: Seismic event locations in relation to the well and inferred orientation of the injection plane.

To quantify seismic activity, we calculate the hypocenter density, as suggested by Dempsey et al. (2016). This measure was developed in an analysis of seismicity at another Australian EGS site in the Cooper Basin, Habanero. As for Habanero, an areal density is computed in accordance with the approximately planar shape of the seismic cloud.

Following Dempsey et al. (2016), we assume that pressure change and hypocenter density are proportional, related by the coefficient of proportionality m_1. This is most probably an oversimplification: the true relation is likely to contain non-linearities given the complex failure mechanisms and heterogeneities involved. Nevertheless, the assumption provides a first order estimate and is a useful starting point for inferring the nature of permeability enhancement.

We do not distinguish events triggered by pressurization and aftershocks from prior earthquakes, which would be decoupled from changes in pressure or temperature. We also do not consider pressure leak off in the rock matrix perpendicular to the plane of injection, which could activate other fractures (with some time delay that would have to be modelled). For simplification, the hypocenter density calculation and modelling assume radial symmetry about the injection well.

A Darcy flow model is constructed to simulate the radial pressure distribution that develops during the stimulation. This model has to satisfy two constraints: injectivity evolution with time, and pressure proportional to hypocenter density at selected times. A calibrated model then delivers the most likely permeability evolution scenario for the Paralana-2 stimulation.

In Section 2, we present the methodology used to calculate hypocenter density. In Section 3, we present the model and its calibration. In Section 4, we discuss the implications for the mechanisms at the origin of permeability changes.

2. HYPOCENTER DENSITY CALCULATION

We use a relocated catalog of 4753 events with magnitudes between -0.6 and 2.6. From these, we use only the 3809 events larger than the magnitude of completeness, M_c = 0.1. The seismic cloud indicates a subhorizontal plane at a depth of around -3800 m, striking at N75E and dipping 13.5°. Most of the significant events are within 70 m of the plane.

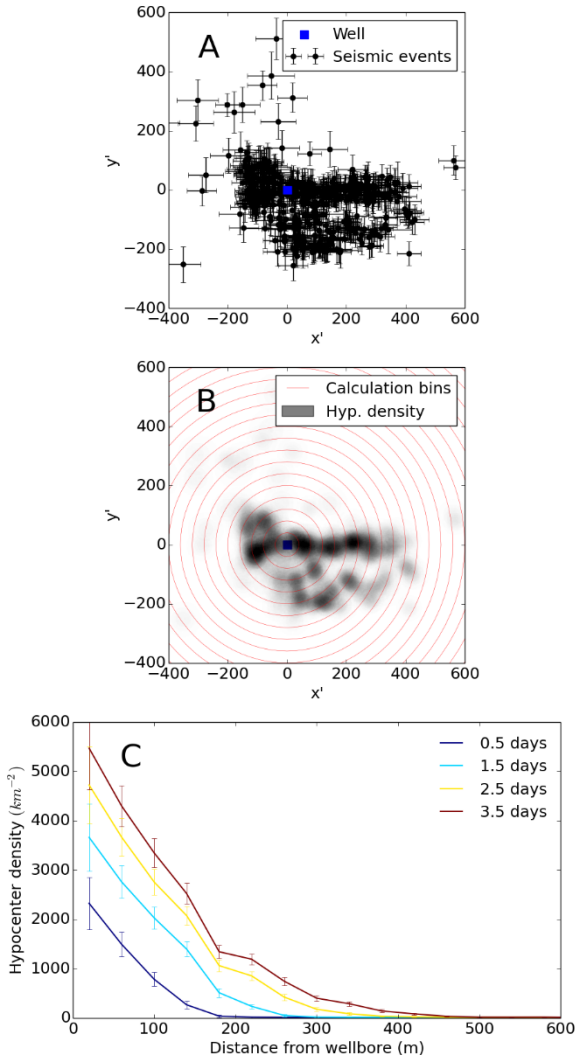

Figure 3: (A) Position of the seismic events with their respective horizontal error in the injection plane adapted base (x', y'), (B) Calculated hypocenter density and radial bins used to establish hypocenter density profiles, (C) Hypocenter density vs distance from the wellbore at four different times.

Each event is associated with a horizontal and vertical error (Fig. 3A), which vary between 40 and 80 m. We apply a normal distribution f to obtain a spatial probability distribution of the event location.

$$f(x,y,z) = \frac{1}{\sqrt{(2\pi)^3\sigma_r^2\sigma_z}}\exp\left(\frac{1}{2}\left[\frac{(x-x_s)^2+(y-y_s)^2}{\sigma_r^2} + \frac{(z-z_s)^2}{\sigma_z^2}\right]\right), \quad [1]$$

where x, y, z are coordinates of a point in space, x_s, y_s, z_s are the coordinates of the hypocenter, all in the original base (Easting, Northing, Altitude). σ_r and σ_z are half of the horizontal and vertical uncertainty in hypocenter location, respectively.

We consider a new base (x', y', z') aligned with the plane of injection with its origin at the wellbore. z' is the normal to the plane, while x' is the intersection of the plane and the horizontal. We construct volumes of integration in this base, cylinders with their axis along z' encompassing the volume between the radiuses r_1 and r_2 and the perpendicular distances $-\frac{h}{2}$ and $\frac{h}{2}$, h being the width of the injection layer. The probability p of a hypocenter to be within the volume of injection defined by r_1 and r_2 is:

$$p(r_1, r_2) = \int_{z'=-\frac{h}{2}}^{z'=\frac{h}{2}} \int_{r'=r_1}^{r'=r_2} \int_{\theta'=0}^{\theta'=2\pi} f(x,y,z) r' \, d\theta' dr' \, dz \qquad [2]$$

where r' and θ' are the polar coordinates the (x', y', z') base. To get the hypocenter density n at a time t_i in the cylinder defined by r_1 and r_2, we sum p of each MEQ that occurred before t_i and divide by the planar area of the integration volume:

$$n(r_1, r_2, t_i) = \frac{1}{\pi(r_2^2 - r_1^2)} \sum_{i=0}^{N(t<t_i)} p(r_1, r_2) \qquad [3]$$

where N is the number of events that occurred before t_i. This calculation is represented graphically on Fig. 3B. The standard deviation, σ, is given by:

$$\sigma(r_1, r_2, t_i) = \frac{1}{\pi(r_2^2 - r_1^2)} \sqrt{\sum_{i=0}^{N(t<t_i)} p(r_1, r_2)\big(1 - p(r_1, r_2)\big)} \qquad [4]$$

We choose bins for r_1 and r_2 as well as t_i to obtain the radial hypocenter density profiles presented in Fig. 3C. Near the well, we observe that hypocenter density is sharply rising in the first half day, before increasing at a steadier rate for the next three days. This implies sustained pressure increase in the near wellbore region according to the assumption that seismicity density is a proxy measure of pore pressure. Further away, we identify an expanding seismicity front. This is a consequence of the fluid spreading through the formations, corresponding to a pore pressure front, as injection continues.

3. RADIAL MODEL

Here, we model the radial distribution of fluid pressure, given different scenarios for permeability evolution. Our goal is to find a scenario that produces an injectivity evolution consistent with observation, and with radial pressure profiles consistent with the hypocenter density computed in Section 2, accounting for some proportionality coefficient m_1.

We use the reservoir simulator FEHM (Zyvoloski, 2007), which implements the control volume method to solve mass and energy conservation in a porous medium. We use a radial geometry, representing the formations in the base (r', z'), with the wellbore at the center. Each block is 35 m thick along z', and 1 m thick radially. At the center, we apply a constant pressure source, fixed at the estimated downhole pressure, 99MPa. A no flow condition is applied at the model boundaries. The model is large enough (1200 m) that pressure changes at the radial boundaries are negligible. The initial pressure is set at 30 MPa.

According to our inverse modelling approach, permeability is prescribed in our flow model. We use a function that covers a wide range of possible configurations for permeability enhancement, while limiting the number of parameters: these are (i) the initial permeability K_0; (ii) the permeability multiplier giving the maximum permeability enhancement, dk; (iii) α, which controls the shape of the permeability radial profile (Fig. 4A); and (iv) β, which controls the speed of the permeability front as it propagates away from the wellbore (Fig. 4B).

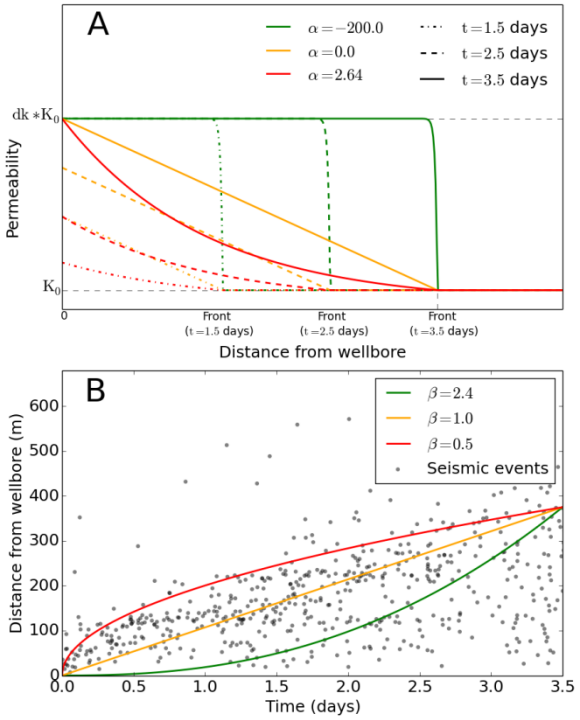

Figure 4: Influence of (A) α and (B) β on the prescribed permeability profiles.

The following equations govern the front position and the permeability profiles:

$$r_{front}(t) = r_{max}\left(\frac{t}{t_{max}}\right)^{\beta} \qquad [5]$$

$if\ \alpha \neq 0$

$$K(r,t) = K_0\left[1 + (dk-1)\frac{e^{\alpha\left(-\frac{r}{r_{max}}+\left(\frac{t}{t_{max}}\right)^{\beta}\right)}-1}{e^{\alpha}-1}\right] \qquad [6]$$

$if\ \alpha = 0$

$$K(r,t) = K_0\left[1 + (dk-1)\left(-\frac{r}{r_{max}} + \left(\frac{t}{t_{max}}\right)^{\beta}\right)\right] \qquad [7]$$

where r_{front} is the distance of the front from the wellbore at the time t, K is the permeability at radial distance r and time t, and r_{max} is the front at the time t_{max}.

Our first objective is to match the injectivity evolution with time. We use α as a fixed parameter, and β, K_0, dk, and the porosity φ as calibration parameters. We use the model analysis python toolkit MATK (http://matk.lanl.gov) which implements a Levenberg-Marquardt algorithm for automated calibration. We set as a calibration target that flow rate increases at a constant rate with time. For each given α, we find parameters giving a satisfying match of the injectivity increase rate. The different calibrated variables are listed in Table 1 and plotted in Fig. 5. It is clear that a number of parameters sets can produce a model that replicates linear injectivity increase at Paralana. Thus another criterion is needed to choose between these permeability models.

Table 1: Calibrated parameters for three scenarios.

α	β	log10(K_0)	dk	φ (%)
-200	2.25	-15.25	11.2	2
0	1.00	-15.44	15.8	10
2.64	0.51	-15.44	15.8	10

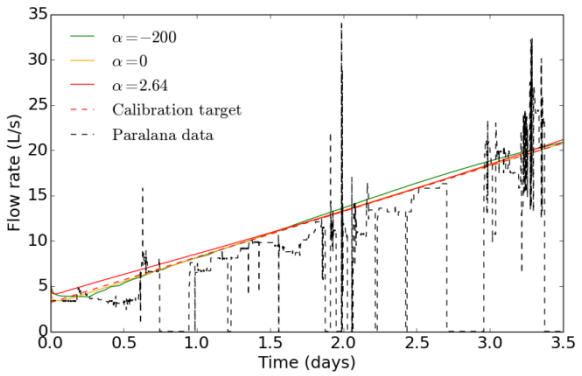

Figure 5: Simulated injection rate for three calibrated scenarios presented in Table 1.

For the first scenario, α = -200, permeability is effectively a step function and assumes two values: K_0 and $dk*K_0$. As the stimulation proceeds, pore pressure near to the wellbore decreases with time. This is because, for constant (but enhanced) permeability, a steepening pressure gradient is needed to achieve increasing injectivity, as shown in Dempsey et al. (2015). Since wellbore pressure is fixed, a dropping pressure near the wellbore is required to achieve the decreasing steeper gradient (Fig. 6A). In the second scenario, α = 0, permeability is linearly increasing with distance and time, as β =1. Because of permeability increase close to the wellbore, a rising injection rate is sustained with an increasing pore pressure throughout the domain (Fig. 6B). When α is increased up to 2.64, pore pressure near the wellbore increases further (Fig. 6C).

Our goal is to find the permeability enhancement scenario that produces simulated pressure profiles that conform as close as possible to the hypocenter density profiles obtained in section 2. We have assumed that induced seismicity is a proxy measure of pore pressure increase, as described in section 1. Once again, automated calibration is applied, this time to obtain values for α and m_1, the proportionality coefficient between pressure and hypocenter density. We aim to match the hypocenter density and pore pressure radial profiles at four different times, 0.5, 1.5, 2.5, 3.5 days. The best calibration is obtained for α = 2.64 (Fig. 7). The best fit value for m_1 is 161 events/km^{-2} MPa^{-1}, which is close to the value of 154 events/km^{-2} MPa^{-1} obtained by Dempsey et al. (2016) for the Habanero#1 stimulation (the datasets have a similar magnitude of completeness, so the quantities are directly comparable). This is remarkable given a different conceptual model for reservoir stimulation: assumption of 2D radial flow but with a fixed permeability field (reflecting enhancement near the wellbore) that does not change in time. Dempsey et al. (2016) used a threshold pressure P_0 above ambient reservoir to fit the seismicity. Aside from these differences, the good agreement between the two m_1 values suggests the assumption that hypocenter density is a proxy measure for pressure change is perhaps quite reasonable.

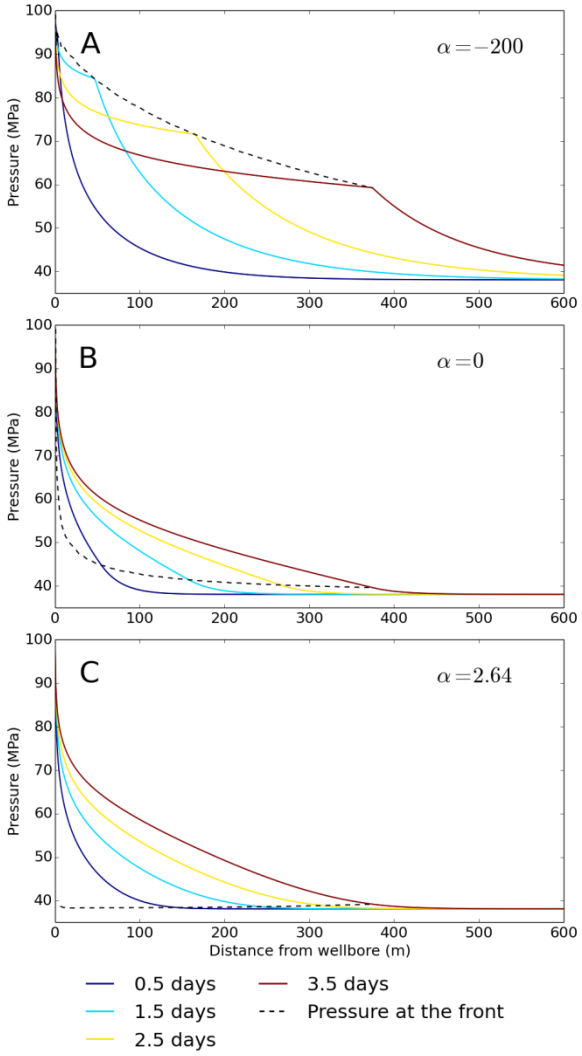

Figure 6: Simulated radial pore pressure profiles at four different times for (A) α = -200, (B) α = 0, and (C) α = 2.64.

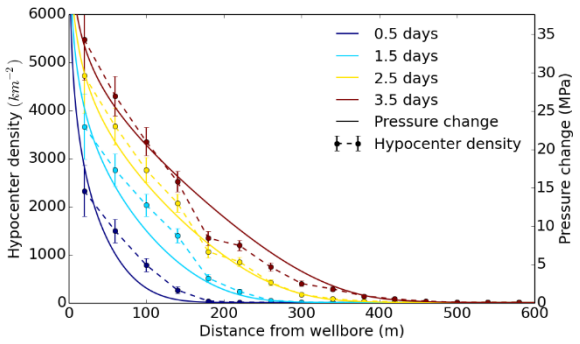

Figure 7: Radial hypocenter density and simulated pressure change profiles at four different times for α = 2.64.

4. PERMEABILITY ENHANCEMENT MECHANISM

While we have elected to prescribe rather than model the enhancement of permeability, we can still gain some insight into the mechanisms responsible by looking at its relationship with the evolving fluid pressure.

As mentioned in Section 1, thermal effects can theoretically modify permeability, either through thermal contraction that dilates fracture apertures or by modifying stresses to promote shear failure. In the Paralana-2 stimulation, fluid was injected at a temperature about 170°C cooler than the rocks in the target layer. Still, significant cooling of formations can be a long process, because the injected fluid heats up as is travels down the wellbore and therefore enters the formation at a higher temperature than at the surface. Simulations in a non-isothermal model, similar to the one presented in Section 3, coupled with a coarse wellbore simulator, indicate that the Paralana-2 stimulation parameters set do not enable significant cooling of formations. Finer simulations including stress calculations would be needed to validate this conclusion but, at this stage, we consider thermal effects an unlikely cause of permeability enhancement.

Close to the wellbore, permeability is affected by both acid injection and shear failure due to pressurization. Continuously increasing permeability close to the wellbore observed in our calibrated model (Fig. 4A, α = 2.64) is not complemented by a similar increase in pore pressure, which tends to approach equilibrium. This suggests that permeability enhancement near the wellbore may be primarily driven by the acid injections.

Further from the wellbore, the mechanisms likely to impact permeability substantially are shear failure driven by poroelastic stress changes or pressurization. For the three simulations in Fig. 6, we track the fluid pressure at the permeability front as it travels into the rock (recall, the permeability front is prescribed by Eq [5] and is not "driven" by pressure). If pressurization is the only mechanism responsible for permeability enhancement, then we would expect the pressure to be approximately constant at the front, i.e., pressure must increase to a threshold before permeability enhancement occurs. Poroelasticity can inhibit or promote shear failure depending on the orientation of stress, the relative position of the pressure/temperature plume, and other parameters (Segall & Lu, 2015). This mechanism might account for small changes in the pressure at the front, although its magnitude is likely small compared to direct pressurization (Riffault et al., 2016).

For α = -200, the front pressure decreases rapidly with time (Fig. 6A). If we consider permeability as a function of pressure in this case (step model), then permeability increases to the enhanced value when pore pressure exceeds a certain threshold. This problem has been solved analytically and gives the solution β = 0.5 (Barenblatt, 1996). It corresponds to a linear increase in the damaged volume (the volume in which permeability has been enhanced), which evolves with the square of r_{front}, in $\sim t^{2\beta}$. In our radial model, these parameters do not correspond to an increase in the injectivity. A front expansion with β = 2.25 was found necessary to simulate the correct injectivity increase, which instead gives a damaged volume expanding at $\sim t^{4.5}$. Both the front pressure and damaged volume evolution make this scenario unlikely to reflect physical processes occurring in Paralana-2.

For the case of α = 0, our model indicates a gently decreasing front pressure (Fig. 6B), while α = 2.64 corresponds to a slightly increasing one (Fig. 6C). As our calibration criteria based on the distribution of seismicity indicated that α = 2.64 is the most likely scenario, it is possible that poroelasticity played an inhibiting role increasing with time in stimulation (accounting for the increased front pressure with time). We note that in the α = 2.64 case, the front pressure is very close to the initial reservoir pressure, which implies that the pressure increase to initiate permeability enhancement is quite low.

The occurrence of MEQs far from the main seismic cloud (Fig. 2) suggests that poroelastic effects, which propagate rapidly ahead of the pressure front, may be operating. Combined with the low pressure threshold needed for permeability enhancement, both features suggest that the crust is critically stressed: a small pressure or stress perturbation can induce shear failure of an existing fracture. In the Habanero#1 stimulation studied by Dempsey et al. (2016), no similar distant events were recorded. Their hypocenter density analysis suggested that a threshold pressure increase of ~5 MPa was required before MEQs were triggered. This indicates that either the crust at the Habanero location is less critically stressed, or that the main fracture plane is less well oriented than at Paralana.

5. CONCLUSION

Using radial Darcy flow models, we have shown that multiple permeability enhancement scenarios can sustain a linearly increasing injection rate at constant wellhead pressure, as approximately occurred during the 2011 Paralana-2 stimulation. These scenarios range from a single step permeability increase with a damaged volume expanding according to $\sim t^{4.5}$, to exponentially increasing permeability and a damaged volume that increases linearly with time.

We assume that induced seismicity reflects subsurface fluid pressure increase. Indeed, shear failure of existing fractures triggered by fluid pressurization is the commonly assumed mechanism behind induced seismicity. To include this in our model, we calculated the density of MEQ hypocenters at different radial distances from the wellbore and at different times (allowing for uncertainty in the hypocenter locations). This information was used to calibrate the model and find the best match between the seismicity and the

pressure profiles. We found that the extreme case of an exponentially increasing permeability with time was the best fit. Step permeability models do not allow for pressure increase near the wellbore and therefore cannot account for ongoing seismic activity in this region (as is the case for Paralana.

Close to the wellbore, permeability enhancement appears decoupled from the pressurization mechanism, as the calibrated model suggests that pressure equilibrates while permeability increases exponentially. One possibility is that recurrent acid injections are the continuing to improve permeability in this region.

Further from the wellbore, pressurization is most likely the dominant mechanism causing permeability enhancement. Pressure plotted at the propagating permeability front indicates that poroelasticity may play a minor role inhibiting shear failure.

The low front pressure, combined with the presence of induced seismic events (presumably poroelastic) at early time and far from the main cloud, indicates that the crust at Paralana is critically stressed: only small pressure or stress perturbations are required to trigger shear failure.

To further explore these ideas, modelling using FEHM's coupled stress capabilities will be performed.

ACKNOWLEDGEMENTS

Funding for this work was provided by the Center for Space and Earth Sciences at Los Alamos National Laboratory, NM, USA. The authors wish to thank Dr Betina Bendall from the Department of State Development of South Australia and Dr. Julie Albaric from Université de Franche-Comté, France, for providing data and insight on the Paralana stimulation.

REFERENCES

Albaric, J., Oye, V., Langet, N., Hasting, M., Lecomte, I., Iranpour, K., Messeiller, M. and Reid, P.: Monitoring of induced seismicity during the first geothermal reservoir stimulation at Paralana, Australia, *Geothermics*, 52, pp.120-131.3. (2014).

Barenblatt, G.I.: Scaling, Self-Similarity, and Intermediate Asymptotics. *Cambridge University Press, Cambridge.* (1996).

Dempsey, David, et al.: Numerical modeling of injection, stress and permeability enhancement during shear stimulation at the Desert Peak Enhanced Geothermal System, *International Journal of Rock Mechanics and Mining Sciences 78*, 190-206. (2015).

Dempsey, D., Barton, C. and Catalinac, A.: Density of induced earthquake hypocenters as a proxy for pore pressure increase during well stimulation, *American Rock Mechanics Association 13-217*. (2016).

Lee, H.S. and Cho, T.F.: Hydraulic characteristics of rough fractures in linear flow under normal and shear load, *Rock Mechanics and Rock Engineering*, 35(4), pp.299-318. (2002).

Majer, E.L., Baria, R., Stark, M., Oates, S., Bommer, J., Smith, B. and Asanuma, H.: Induced seismicity associated with enhanced geothermal systems, *Geothermics 36*, no. 3: 185-222. (2002).

Petraterm: Paralana 2 Stimulation Treatment (July 2011). (2012).

Riffault, J., Dempsey, D., Archer, R., Kelkar, S. and Karra, S.: Understanding Poroelastic Stressing and Induced Seismicity with a Stochastic/Deterministic Model: an Application to an EGS Stimulation at Paralana, South Australia, 2011, *Proceedings, forty-first Workshop on Geothermal Reservoir Engineering*, Stanford. (2016).

Segall, P. and Lu, S.: Injection-induced seismicity: Poroelastic and earthquake nucleation effects, *Journal of Geophysical Research: Solid Earth*, 120(7), pp.5082-5103. (2015).

Tester, J.W., Anderson, B.J., Batchelor, A.S., Blackwell, D.D., DiPippo, R., Drake, E.M., Garnish, J., Livesay, B., Moore, M.C., Nichols, K. and Petty, S: The future of geothermal energy, Impact of Enhanced Geothermal Systems (EGS) on the United States in the 21st Century, Massachusetts Institute of Technology, Cambridge, MA 372. (2007).

Zyvoloski, G.: FEHM: A control volume finite element code for simulating subsurface multi-phase multi-fluid heat and mass transfer, *Los Alamos Unclassified Report* LA-UR-07-3359. (2007).